

Covariate Connectivity Combined Clustering for Weighted Networks

Zeyu Hu¹, Wenrui Li¹, Jun Yan¹, and Panpan Zhang^{2,*}

¹Department of Statistics, University of Connecticut, Storrs, CT 06269

¹Department of Biostatistics, Vanderbilt University Medical Center,
Nashville, TN 37203

^{*}Correspondence: [Panpan Zhang](#)

November 24, 2025

Abstract

Community detection is a central task in network analysis, with applications in social, biological, and technological systems. Traditional algorithms rely primarily on network topology, which can fail when community signals are partly encoded in node-specific attributes. Existing covariate-assisted methods often assume the number of clusters is known, involve computationally intensive inference, or are not designed for weighted networks. We propose C^4 : Covariate Connectivity Combined Clustering, an adaptive spectral clustering algorithm that integrates network connectivity and node-level covariates into a unified similarity representation. C^4 balances the two sources of information through a data-driven tuning parameter, estimates the number of communities via an eigengap heuristic, and avoids reliance on costly sampling-based procedures. Simulation studies show that C^4 achieves higher accuracy and robustness than competing approaches across diverse scenarios. Application to an airport reachability network demonstrates the method's scalability, interpretability, and practical utility for real-world weighted networks.

Key words. community detection; covariate-assisted learning; network analysis; spectral clustering; similarity fusion; tuning parameter selection

1 Introduction

Community detection is a central problem in network analysis that seeks to identify groups of nodes that are densely interconnected or share similar attributes within a larger network (Girvan and Newman, 2002; Fortunato, 2010). Uncovering such communities reveals the organizational structures or functional modules that govern complex systems. In social networks, community detection has been widely used to analyze collaboration and interaction patterns (Barabási et al., 2002; Handcock et al., 2007; Ji et al., 2022), with methodological advances further enhancing the modeling of such structures (Ouyang et al., 2021, 2023). In biological systems, modular organization plays a fundamental role in processes such as brain function (Sporns and Betzel, 2016). In technological and information networks, community detection supports the analysis of incomplete or large-scale structures (Lin et al., 2012). Applications also extend to public health, where clustering methods have been employed to group states by disease dynamics and to model covariate-assisted network structures (Chen and Zhang, 2022; Louit et al., 2025). The ubiquity of network data across these diverse domains underscores the importance of developing reliable community detection methods to uncover hidden structures and gain insights into the organization and function of real-world systems.

Classical community detection methods primarily rely on network topology. Modularity optimization approaches, including the Girvan–Newman algorithm and its successors (Girvan and Newman, 2002; Newman and Girvan, 2004; Newman, 2006), remain influential for their ability to reveal cohesive modules in networks, with the Louvain method especially popular for its efficiency and scalability on large graphs (Blondel et al., 2008). Spectral clustering methods exploit the eigenspectrum of graph Laplacians to identify low-dimensional embeddings of network structure (Shi and Malik, 2000; Ng et al., 2002; von Luxburg, 2007), while other graph-based strategies include edge betweenness (Radicchi et al., 2004), random-walk methods (Pons and Latapy, 2005; Rosvall and Bergstrom, 2008), and label propagation (Raghavan et al., 2007). Probabilistic formulations such as the mixed-membership

stochastic block model extend this topological perspective (Airoldi et al., 2008). These methods effectively detect well-separated clusters but struggle when relevant signals are not fully encoded in connectivity alone, motivating the use of node attributes to enhance community detection.

Covariate-assisted methods extend community detection by combining network topology with node attributes. Covariate-assisted spectral clustering (CASC) integrates connectivity and attributes but requires the number of communities to be specified in advance (Binkiewicz et al., 2017). To improve performance in sparse networks, regularization strategies have been proposed to stabilize estimation (Yan and Sarkar, 2021). Bayesian frameworks offer complementary strategies. Tallberg (2004) introduced one of the earliest covariate-dependent block models, and Newman and Clauset (2016) formalized inference in annotated networks. Recent developments extend the stochastic block model to incorporate covariates via random partition models (Shen et al., 2025), latent factor formulations (Louit et al., 2025), and multilayer settings (Contisciani et al., 2020; Xu et al., 2023). Empirical applications also demonstrate the utility of attributes, such as in collaboration networks of statisticians (Zhang et al., 2023). Despite these advances, no existing method efficiently integrates weighted network structure with informative covariates while jointly balancing the two information sources and determining the number of communities in a fully data-driven manner.

To fill this gap, we propose Covariate Connectivity Combined Clustering (C^4), a simple yet effective algorithm that fuses network connectivity with node covariates. The method jointly incorporates weighted network structure and informative node attributes, adaptively selects the tuning parameter that balances these two sources of information, and determines the number of communities in a data-driven manner. In contrast to existing Bayesian formulations, C^4 avoids reliance on computationally intensive Markov chain Monte Carlo procedures and remains highly scalable. Through extensive simulations, we show that C^4 achieves higher clustering accuracy and robustness than competing methods across a wide range of network configurations, both when the number of communities is known and unknown. Ap-

plication to an airport reachability network reveals geographically coherent and demographically meaningful communities, further demonstrating its scalability and interpretability,. Together, these results establish C^4 as a practical and robust solution for covariate-assisted community detection in weighted networks.

The remainder of the paper is organized as follows. Section 2 details the proposed C^4 algorithm, including the construction of the covariate-based similarity matrix, the fusion of connectivity and covariate information, the selection of the tuning parameter, and the practical implementation. Section 3 reports simulation studies conducted under both known and unknown community numbers, evaluating the accuracy and robustness of C^4 across a variety of network configurations. Section 4 presents an application to an airport reachability network, illustrating the scalability and interpretability of the method in practice. Section 5 discusses the limitations and future directions.

2 Method

We begin with introducing notations for weighted networks and covariates (Section 2.1). Then, we detail how connectivity and covariate information are fused within a spectral clustering framework (Section 2.2) and describe the procedure for selecting the tuning parameter (Section 2.3). Implementation details are provided in Section 2.4.

2.1 Notations

We first introduce notations for the weighted network and node-level covariates. Let $G := G(V, E)$ represent a weighted, undirected network with node set V and edge set E . Let $|V| = n$ be the number of nodes in G . The structure of G is characterized by a weighted adjacency matrix $\mathbf{W} := (w_{ij})_{n \times n}$, where w_{ij} is the weight between nodes $i, j \in V$. If nodes i and j are not connected, then we set $w_{ij} = 0$. Further, we do not consider self-loops by enforcing $w_{ii} = 0$ for all $i \in V$. For each node i , let $z_i \in \{1, 2, \dots, K\}$ denote its community label,

where K is the total number of communities. Collectively, $\mathbf{z} = (z_1, z_2, \dots, z_n)^\top$ represents the clustering assignment of all nodes. In practice, K is unknown.

Each node i is endowed with a p -dimensional covariate vector \mathbf{X}_i collecting the node-level features. Let $f := \mathbb{R}^p \times \mathbb{R}^p \mapsto \mathbb{R}$ be a similarity function that quantifies the closeness between \mathbf{X}_i and \mathbf{X}_j for each pair of $i, j \in V$, with larger values indicating greater similarity. Distances followed by inverse transformations are commonly used: Euclidean distance for continuous variables, Hamming distance for categorical variables, and more flexible metrics such as Gower's distance for mixed data (Wang et al., 2021). The choice of inverse transformation depends on both the selected distance function and the practical interpretation of the real data. Let $\mathbf{S} := (s_{ij})_{n \times n}$ denote the similarity matrix, with $s_{ij} = f(\mathbf{X}_i, \mathbf{X}_j)$.

2.2 Covariate Connectivity Combined Clustering

Our C⁴ integrates network topology and node-level covariates within a spectral clustering framework. This methods enables uncovering communities that are not only structurally cohesive but also homogeneous with respect to relevant nodal attributes. Define $\mathbf{C} := (c_{ij})_{n \times n} = (1 - \alpha)\mathbf{W} + \alpha\mathbf{S}$, where $\alpha \in [0, 1]$ is a tuning parameter balancing the structural and covariate similarity. Setting $\alpha = 0$ reduces to structure-only clustering, while $\alpha = 1$ refers to covariate-only clustering. Intermediate values of α fuse the two information sources. Because \mathbf{W} and \mathbf{S} may differ in scale, we rescale \mathbf{S} so that its total sum matches that of \mathbf{W} :

$$\mathbf{S} \leftarrow \mathbf{S} \times \frac{\sum_{i,j} w_{ij}}{\sum_{i,j} s_{ij}}. \quad (1)$$

This adjustment ensures that neither source dominates due to magnitude differences.

For any fixed choice of α , spectral clustering is performed on the normalized Laplacian of \mathbf{C} :

$$\mathbf{L}_{\text{norm}} = \mathbf{I} - \mathbf{D}^{-1/2} \mathbf{C} \mathbf{D}^{-1/2}, \quad (2)$$

where \mathbf{I} is the identity matrix, and \mathbf{D} is a diagonal matrix with $d_{ii} := \sum_{j=1}^n c_{ij}$. Spectral

clustering interprets community detection as an eigenvalue problem, embedding nodes in the eigenspace of \mathbf{L}_{norm} (Chung, 1997; Ng et al., 2002; von Luxburg, 2007). Communities are then identified using k -means applied to the eigenvectors corresponding to the smallest eigenvalues. The number of clusters K is chosen adaptively via an eigengap heuristic (Ng et al., 2002). Specifically, if $\lambda_{(1)}, \lambda_{(2)}, \dots, \lambda_{(n)}$ are the ordered eigenvalues of \mathbf{L}_{norm} , we set

$$K = \arg \max_{k \in \{2, \dots, n-1\}} (\lambda_{(k+1)} - \lambda_{(k)}). \quad (3)$$

The multiplicity of the zero eigenvalue of \mathbf{L}_{norm} equals the number of connected components in the graph. In practice, when the graph is connected, there is a single zero eigenvalue; the eigengap heuristic is applied to the ordered sequence of eigenvalues, including the zero(s).

2.3 Tuning Parameter Selection

The tuning parameter α is selected through a data-driven grid search that maximizes the silhouette score, a distance-based criterion measuring how well nodes are clustered. Since its appearance (Rousseeuw, 1987), the silhouette score has become a standard internal validation criterion because it simultaneously quantifies within-cluster cohesion and between-cluster separation, while not requiring external labels (Shahapure and Nicholas, 2020). Because of its robustness, direct interpretability, and ease of use, the silhouette score has become a prevalent metric for model selection, particularly in clustering research (Dudek, 2020; Januzaj et al., 2023).

To operationalize this selection, the silhouette score is computed from pairwise node distances derived from the fused adjacency-similarity matrix \mathbf{C} . The distance between nodes i and j is defined as $d(i, j) = 1/(c_{ij} + \varepsilon)$, where c_{ij} denotes the integrated similarity in \mathbf{C} and $\varepsilon > 0$ provides numerical stability. This definition ensures that stronger similarities correspond to shorter distances. For each candidate α in the pre-specified grid \mathbb{A} , we construct \mathbf{C} , estimate the number of clusters K by the eigengap heuristic (Section 2.2), and evaluate the

Algorithm 1: Pseudocode for C⁴.

Input: Weighted adjacency matrix \mathbf{W} ; covariate similarity matrix \mathbf{S} ; grid for tuning parameter \mathbb{A} ; number of clusters K_{true} (optional).
Output: Community labels \mathbf{z} ; optimal tuning parameter α_{opt} ; number of clusters K_{opt} (user-provided or data-driven).

```
1 Rescale  $\mathbf{S}$  with Equation (1);
2 foreach  $\alpha \in \mathbb{A}$  do
3   Construct  $\mathbf{C} \leftarrow (1 - \alpha)\mathbf{W} + \alpha\mathbf{S}$ ;
4   Compute the normalized Laplacian  $\mathbf{L}_{\text{norm}}$  of  $\mathbf{C}$  using Equation (2);
5   Calculate and sort the eigenvalues of  $\mathbf{L}_{\text{norm}}$ :  $\lambda_{(1)} \leq \dots \leq \lambda_{(n)}$ ;
6   if  $K_{\text{true}}$  is not null then
7     | Set  $K(\alpha) \leftarrow K_{\text{true}}$ ;
8   else
9     | Set  $K(\alpha) \leftarrow \arg \max_{k \in \{2, \dots, n-1\}} (\lambda_{(k+1)} - \lambda_{(k)})$ ;
10  end
11  Extract community labels  $\mathbf{z}(\alpha)$  by applying the  $k$ -means algorithm to the
    eigenvectors corresponding to  $\lambda_{(1)}, \dots, \lambda_{(K(\alpha))}$ ;
12  Compute the silhouette score  $\text{SilS}(\alpha)$  based on  $\mathbf{C}$  and  $\mathbf{z}(\alpha)$  using distance
     $d(i, j) = 1/(C_{ij} + \varepsilon)$ ;
13 end
14 Set  $\alpha_{\text{opt}} \leftarrow \arg \max_{\alpha \in \mathbb{A}} \text{SilS}(\alpha)$ ,  $\mathbf{z} \leftarrow \mathbf{z}(\alpha_{\text{opt}})$ , and  $K_{\text{opt}} \leftarrow K(\alpha_{\text{opt}})$ ;
15 return  $\mathbf{z}$ ,  $\alpha_{\text{opt}}$ , and  $K_{\text{opt}}$ .
```

silhouette score. The final choice of both α and K are obtained jointly by selecting the pair (α, K) that maximizes the silhouette score.

2.4 Implementation

The pseudocode for C⁴ is provided in Algorithm 1. An open-source and user-friendly R package, **c4**, is available on GitHub. The package provides functions for performing spectral clustering, including the proposed C⁴ and the covariate-assisted spectral clustering (CASC) method by [Binkiewicz et al. \(2017\)](#), along with additional utilities for preprocessing and evaluation. Although several CASC implementations are publicly available, the original **rCASC** codes from [Binkiewicz et al. \(2017\)](#) did not run properly in our experiment, mainly due to incompatibility with updates of several supporting R package. In addition, the **CASC()** function in the **CASCORE** package ([Hu and Wang, 2023](#)) applies only when the covariate

dimension exceeds the number of clusters, which limits its applicability. Hence, we developed our own implementation of CASC in package `c4`, with the full workflow illustrated in a vignette, from data generation and preprocessing to clustering. All random seeds used in our simulations are properly documented to ensure reproducibility.

3 Simulations

Simulation study evaluates the performance of the proposed C^4 method under controlled network topology and covariate signal conditions. The study consists of two parts. The first examines scenarios where the number of clusters K is known, while the second considers a more realistic setting where K is unknown. In both parts, C^4 is compared with two fixed baselines: (1) structure-only clustering, which applies spectral clustering to the weighted adjacency matrix \mathbf{W} (corresponding to $\alpha = 0$); and (2) covariate-only clustering, which applies spectral clustering to the covariate similarity matrix \mathbf{S} (corresponding to $\alpha = 1$). Unlike these baselines, C^4 adaptively selects α from the tuning grid $\mathbb{A} = \{0, 0.1, 0.2, \dots, 1\}$ to optimize clustering performance. When K is known, CASC is included for comparison (Binkiewicz et al., 2017). All simulation codes and random seeds are provided in the online supplements to ensure reproducibility.

3.1 Data Generation

The simulation design systematically varies network size, cluster number, and covariate and structural signal strengths to evaluate C^4 under conditions of increasing difficulty. Networks of size $n \in \{400, 800\}$ were generated with $K \in \{4, 8\}$ communities. The strength of covariate signal was jointly determined by the distances among cluster means and the noise parameter σ . Specifically, each node was associated with a three-dimensional covariate vector ($p = 3$) drawn from a multivariate normal distribution $\text{MVN}(\boldsymbol{\mu}_k, \sigma^2 \mathbf{I})$ if node i belongs to cluster $k \in \{1, 2, \dots, K\}$, where $\boldsymbol{\mu}_k \in \mathbb{R}^3$ denotes the cluster mean and σ controls

within-cluster variability.

The covariate structure controlled overlap among communities through the configuration of cluster centers and the noise parameter σ . When $K = 4$, the cluster centers μ_k corresponded to the four vertices of a regular tetrahedron centered at the origin with fixed edge length 10. When $K = 8$, they were positioned at the eight vertices of a cube centered at the origin with the same edge length. The degree of overlap, and thus the strength of the covariate signal, was determined jointly by the distances between cluster means and the value of σ . We considered $\sigma \in \{2, 3\}$, representing respectively strong and weak separation. Pairwise dissimilarity between nodes was measured by the Euclidean distance, and the similarity matrix \mathbf{S} was defined as $s_{ij} = 1/\|\mathbf{X}_i - \mathbf{X}_j\|_2$ for $i \neq j$ and $s_{ii} = 0$. This design provided continuous covariates with tunable signal strength for evaluating information fusion in clustering.

On the other hand, the strength of the structural signal was controlled by edge probabilities and weights. Specifically, network topology was generated by fixing the within-community edge probability at $b_{\text{win}} = 0.6$ and varying the between-community probability $b_{\text{btw}} \in \{0.3, 0.4, 0.5\}$. Both unweighted and weighted networks were examined. In the weighted case, each edge weight w_{ij} was independently drawn from $\text{Gamma}(2, \theta)$ with $\theta_{\text{btw}} = 1$ for between-community edges and $\theta_{\text{win}} \in \{1, 1.25, 1.5\}$ for within-community edges. Increasing b_{btw} or decreasing θ_{win} weakened the structural contrast between communities, making the clustering problem more difficult. In contrast, larger network size n improved estimation stability and enhanced separation. Each combination of $(n, K, \sigma, b_{\text{btw}})$ and weighting scheme, either unweighted or weighted with a given θ_{win} , was replicated 100 times to ensure reliable comparisons across methods.

3.2 Results

We separately report the results from settings with known K and unknown K .

3.2.1 Known K

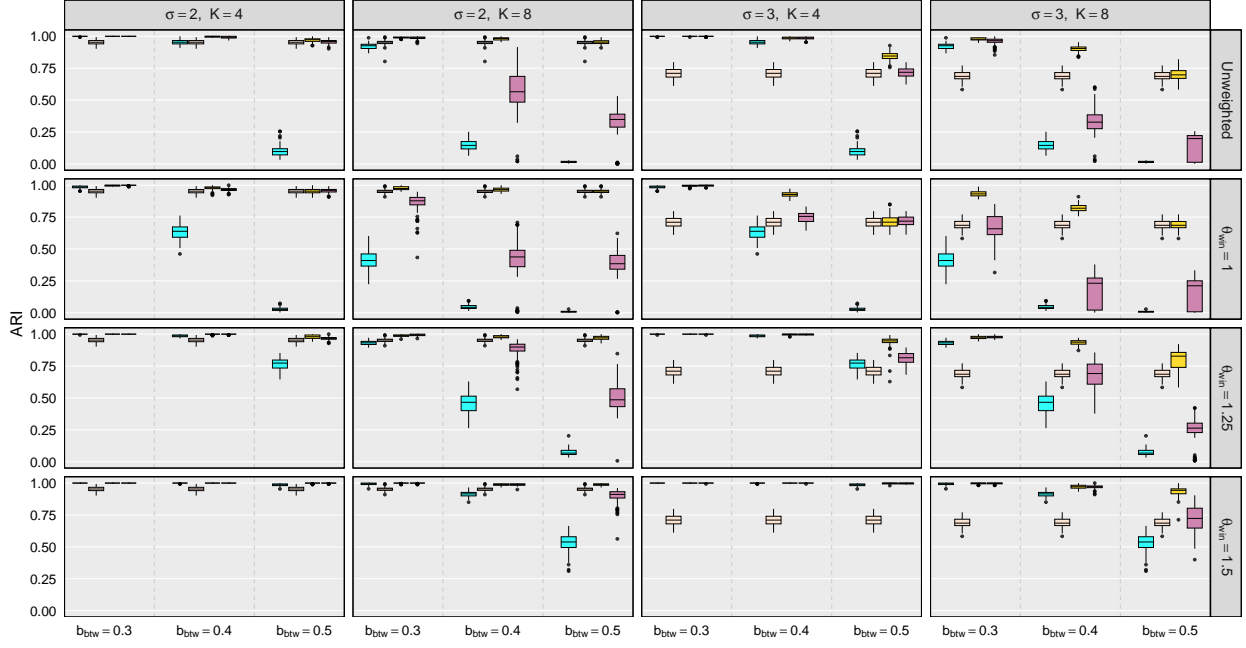
The experiments with known K evaluated how accurately and consistently C^4 recovered community structures when the true number of clusters was provided. Clustering accuracy was measured by the Adjusted Rand Index (ARI, [Rand, 1971](#)), which quantifies agreement between estimated and true community assignments. ARI is unaffected by label switching and remains stable under unbalanced group sizes. Figure 1 displays boxplots of the ARI from 100 replicates under each simulation setting for different methods.

Across all settings, weakening the structural signal lowers accuracy for the baselines, while C^4 remains stable. In unweighted networks, holding σ , n , K and $b_{\text{win}} = 0.6$ fixed, increasing b_{btw} from 0.3 to 0.5 reduces within- and between-community contrast and drives the ARI for $\alpha = 0$ sharply downward in every panel of the top row of Figure 1. CASC tracks C^4 when the structure is strong (e.g., $b_{\text{btw}} = 0.3$) but deteriorates more quickly as b_{btw} grows, with lower medians and greater dispersion. The same pattern appears in weighted networks as θ_{win} decreases. For example, in Figure 1 with $\sigma = 2$, $n = 400$, and $K = 8$, $\alpha = 0$ continues to fall as θ_{win} moves from 1.5 to 1, CASC declines noticeably, and C^4 changes little with small variance. These comparisons imply that CASC is more sensitive to structural weakening, whereas C^4 maintains accuracy and stability.

When the covariate signal weakens, $\alpha = 1$ drops, but C^4 remains stable and often outperforms. Comparing Figure 1 at $\sigma = 2$ versus $\sigma = 3$ with $n = 400$ and $K = 8$, both C^4 and CASC achieve high ARI when the structure is strong (e.g., $\theta_{\text{win}} = 1.5$ with $b_{\text{btw}} \in \{0.3, 0.4\}$), indicating limited sensitivity to covariate noise under dominant structural topology. As structural information becomes limited, increasing σ depresses CASC more than C^4 : medians shift downward and variability grows across all three b_{btw} levels, while C^4 retains higher medians and smaller dispersion. These patterns show that when covariate signal is weaker and structure is not decisive, C^4 better balances the two sources and preserves accuracy.

Larger networks and fewer communities aid all methods, but C^4 continues to lead in median ARI and stability. Gains are evident as n increases or K decreases across panels,

(a) Network size $n = 400$.



(b) Network size $n = 800$.

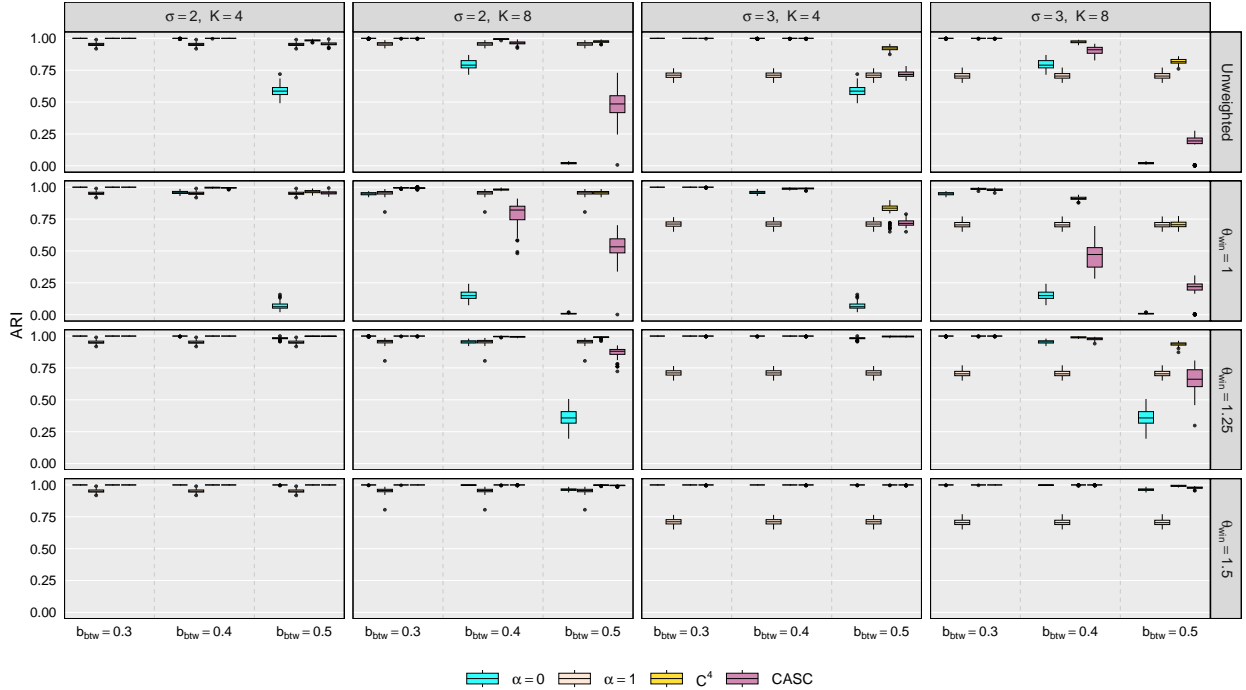


Figure 1: Side-by-side ARI boxplots for known $K \in \{4, 8\}$ with $n = 400$ (upper) and $n = 800$ (lower).

reflecting more stable eigenvectors and easier separation. Notably, under the most extreme setting ($b_{\text{btw}} = 0.5$, $\theta_{\text{win}} = 1$, $K = 8$), the structure provides little usable information; C^4 then selects $\alpha = 1$ and relies on covariates, yielding reasonable clustering despite negligible topology. While such cases are rare in practice, they illustrate the adaptive mechanism: C^4 shifts weight away from uninformative structure to maintain performance.

3.2.2 Unknown K

The next experiment considered the more realistic setting in which the number of communities K was unknown. For each method, K was determined using the eigengap heuristic described in Section 2.2, and clustering accuracy was again evaluated by ARI.

The accuracy of K estimation was examined first. Table 1 presents a representative example with moderate topology structure: $n = 400$, $b_{\text{btw}} = 0.4$, and $K = 8$, using edge weights from a Gamma distribution with scale $\theta_{\text{win}} = 1.25$, a configuration typical of many weighted networks where within-community edges have larger average weights. Results are reported for two levels of the signal-to-noise ratio controlled by $\sigma \in \{2, 3\}$.

Table 1: A summary of the selected community number K for $n = 400$, $b_{\text{btw}} = 0.4$, $\theta_{\text{win}} = 1.25$, and true $K = 8$: Sensitivity to the signal-to-noise ratio $\sigma \in \{2, 3\}$.

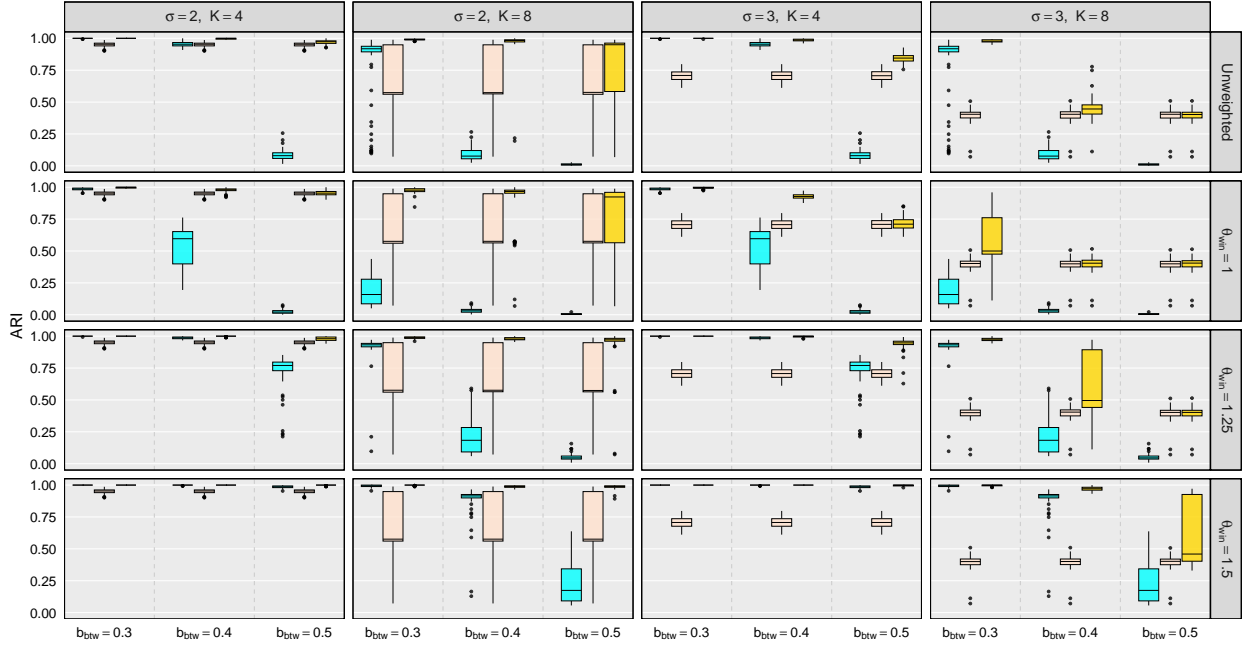
Method	$\sigma = 2$							$\sigma = 3$								
	2	3	4	5	6	7	8	≥ 9	2	3	4	5	6	7	8	≥ 9
$\alpha = 0$	34	20	17	8	11	7	1	2	34	20	17	8	11	7	1	2
$\alpha = 1$	2	0	59	1	0	0	34	4	2	0	95	3	0	0	0	0
C^4	0	0	0	0	0	0	98	2	1	0	56	3	1	7	30	2

The baseline method $\alpha = 0$ underestimates the number of clusters. This poor performance reflects the difficulty of extracting sufficient community information under moderate network structures. When the covariate signal is strong ($\sigma = 2$), $\alpha = 1$ performs reasonably well, correctly identifying $K = 8$ in about one-third of cases, but it also tends to underestimate K . By integrating both structure and covariate information, C^4 achieves near-perfect accuracy, significantly outperforming either baseline. This demonstrates that when both

structure and covariate are informative, C^4 can leverage their complementary strengths to achieve higher accurate K estimation. As the covariate signal weakens to $\sigma = 3$, $\alpha = 1$ exhibits a dramatic decline, with correct estimated K falling to zero. However, C^4 maintains reasonable performance, correctly identifying $K = 8$ in 30% cases. Crucially, the adaptive mechanism of C^4 allows it to compensate for the weakened covariate signal by increasing the weight on structural information. While neither structure alone ($\alpha = 0$) nor covariate alone ($\alpha = 1$) provides accurate K estimation in this challenging scenario, integration of both sources under C^4 yields more reliable results. The patterns observed in Table 1 are consistent among other parameter combinations (see Appendix A for the distributions of K selection), highlighting that the advantage of C^4 in K selection remains stable across different structural and covariate signal strengths.

Clustering accuracy with unknown K remains highest and most stable for C^4 across all simulation settings. Boxplots in Figure 2 show that, although every method suffers some loss of accuracy relative to the known K case (Figure 1), C^4 consistently attains the highest or tied-for-highest median ARI with smaller dispersion. When both structural and covariate information are strong (e.g., $\sigma = 2$, $K = 4$, $n = 400$, $b_{\text{btw}} = 0.3$), C^4 effectively fuses the two sources and matches or surpasses the best baseline performance. When only one source is reliable, either strong topology but weak covariates ($\sigma = 3$) or strong covariates but weak topology ($b_{\text{btw}} = 0.5$), C^4 automatically assigns greater weight to the informative component, maintaining high and stable ARI. Even when both signals are weak, C^4 produces superior accuracy to either baseline alone. Patterns remain consistent across weighted networks and different values of n and K . In extreme configurations characterized by weak structure and noisy covariates ($b_{\text{btw}} = 0.5$, $\sigma = 3$, $K = 8$), C^4 tends to select $\alpha = 1$, effectively reducing to covariate-only clustering; details of these cases and the resulting K distributions are provided in Appendix A.

(a) Network size $n = 400$.



(b) Network size $n = 800$.

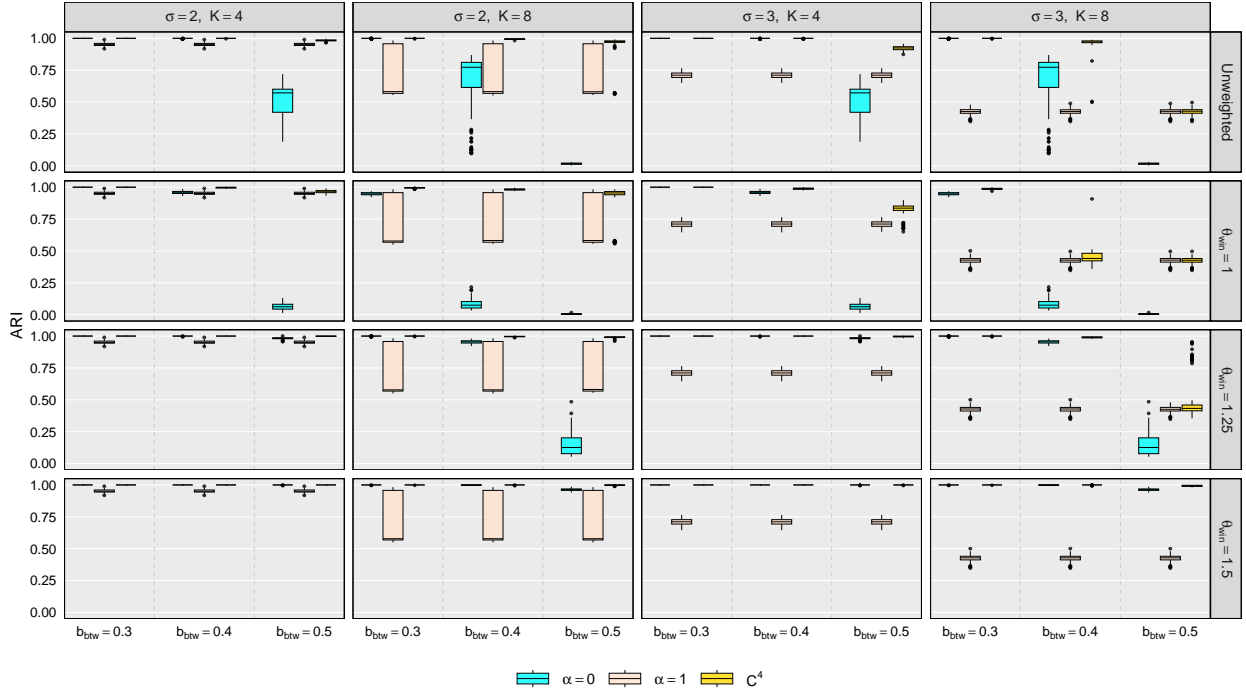


Figure 2: Side-by-side ARI boxplots for unknown $K \in \{4, 8\}$ with $n = 400$ (upper) and $n = 800$ (lower).

4 Application to Airline Reachability Network

We applied our method to an Airline Reachability Network (ARN) dataset (Frey and Dueck, 2007). The dataset captures the reachability relationships among 456 major cities in the United States (including Alaska and Hawaii) and Canada, reflecting how easily each city can be accessed by others in terms of estimated commercial airline travel times. Each node represents a city, and a directed edge from city i to city j is established if the estimated airline travel time from i to j , including expected stopover delays, does not exceed 48 hours. The travel times in ARN range from 10 minutes for short regional flights to nearly 48 hours for the longest multi-leg itineraries. Because airline routes are not always reciprocal and prevailing headwinds cause directional differences in flight durations, the ARN exhibits both structural and weight asymmetries: some city pairs are connected only in one direction due to route availability, and even for bidirectional pairs, the edge weights from i to j and from j to i differ because of flight-time asymmetry. Among the 71,959 directed edges, 34,012 city pairs are bidirectional and 3,935 are unidirectional. Among the bidirectional edges, 98% have different weights.

We construct an undirected, weighted network by including only city pairs that are mutually connected via directed edges. The edge weight is computed as the inverse of the mean bidirectional travel time between nodes i and j so that shorter travel times correspond to stronger connections. The resulting undirected ARN exhibits substantial degree heterogeneity: a small number of hub cities connect to hundreds of cities, whereas most smaller regional cities have only a few connections. Such structural characteristics make the ARN a challenging but informative setting for evaluating our C⁴ method.

We incorporate a single node-level covariate for each city: the logarithm of the surrounding metropolitan population (Benson et al., 2016). Population size captures the scale of travel demand and the relative importance of a city within the airline mobility system, making it a meaningful factor for characterizing node-level heterogeneity. For each city pair, we define similarity as the mean of their log-transformed populations. Using the mean empha-

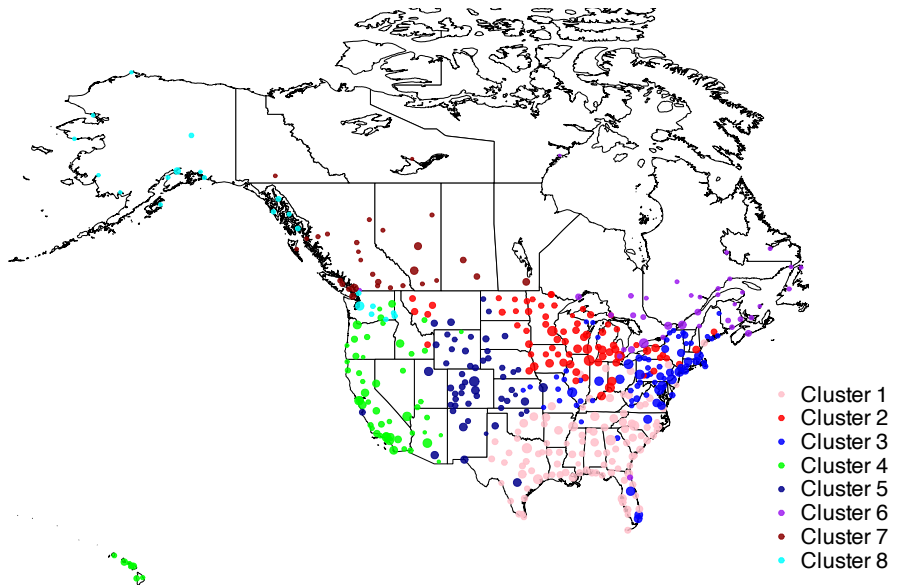


Figure 3: Clustering result based on application of C^4 to the ARN.

sizes the overall market size accessible through a connection and captures the shared demand potential between two cities. This generates a symmetric similarity matrix that serves as the covariate-based input to our method.

Applying the C^4 method to the ARN leads to the optimal tuning parameter $\alpha = 0.4$ and selects $K = 8$ based on the eigengap heuristic. Figure 3 depicts the community structure, with node size proportional to strength (the sum of incident edge weights), revealing geographically coherent clusters. For clarity, edges between nodes are omitted in Figure 3. Table 2 reports each cluster's size, largest city (by node strength), and median metropolitan population, while Table 3 presents both within- and between-cluster densities, defined as the proportion of observed edges among all possible node pairs, with clusters denoted by C-1 to C-8. The results highlight four key characteristics driven by population scale and connection intensity: (1) Clusters 1–2 contain large metropolitan areas such as Atlanta and Chicago, combining high population with strong internal ties that form national travel corridors; (2) Clusters 3–4 include major cities such as Washington DC, New York, Phoenix, and Los Angeles, representing equally large markets but lower densities due to wide geographic span; (3) Clusters 5, 7, and 8 comprise metropolitan cities such as Denver, Vancouver, and Seattle.

Table 2: Summary of community properties of airports across the U.S. and Canada, including community size, largest city (in terms of node strength), and metropolitan population median.

	Size	Largest City	Population Median
Cluster 1	106	Atlanta, GA	357,728
Cluster 2	75	Chicago, IL	187,612
Cluster 3	74	Washington, DC	133,310
Cluster 4	59	Phoenix, AZ	211,888
Cluster 5	54	Denver, CO	46,388
Cluster 6	37	Toronto, ON	53,100
Cluster 7	29	Vancouver, BC	46,850
Cluster 8	22	Seattle, WA	13,732

Table 3: Within- and between-community densities (in percentage) based on the clustering result.

	C-1	C-2	C-3	C-4	C-5	C-6	C-7	C-8
C-1	67	47	39	35	29	14	11	11
C-2		68	36	33	33	16	16	14
C-3			47	29	24	22	12	13
C-4				54	45	12	22	36
C-5					71	8	15	15
C-6						45	28	5
C-7							68	14
C-8								71

that (though not as large as New York or Los Angeles) exhibit high internal cohesion.; and (4) Cluster 6, with Toronto among its largest members, spans distant Canadian provinces and exhibits the weakest internal linkage. Overall, the C⁴ results show that population scale and connectivity intensity are not aligned and that the method effectively disentangles these two structural dimensions of the airline network.

Clusters 1–4 contain populous U.S. regions that anchor the national air-transportation system but differ markedly in their internal connectivity. Cluster 1, centered on Atlanta, the largest city in the group, extends through the Southeast and into the eastern Midwest, while Cluster 2, led by Chicago, links central U.S. markets with the East Coast. In contrast, Cluster 3 comprises several global metropolitan centers including Washington DC, New York,

Philadelphia, and Boston, yet extends southward to tourism-linked cities such as Orlando and Miami. Cluster 4, encompassing Phoenix, Los Angeles, Las Vegas, San Francisco, and tourist destinations in Hawaii, comprises major metropolitan areas in the western region and exhibits a hub-dominated structure.

Clusters 5–8 represent smaller but more cohesive regional systems, largely situated in the Mountain West and adjacent western regions of the United States and Canada. Clusters 5, 7, and 8 share a common pattern of compact geography and strong internal ties despite modest population size. Cluster 5, centered on Denver, connects numerous Rocky Mountain cities into a dense network. Cluster 7, dominated by Vancouver, forms a tightly connected western Canadian region, and Cluster 8 links Seattle with airports in Alaska and the Pacific Northwest, making it the smallest yet most internally connected community. In contrast, Cluster 6, with Toronto as its largest city, spans central Canadian provinces, reflecting long distances between major population centers therein. These patterns demonstrate that compact geography, rather than market size, drives cohesion, a distinction the C^4 method captures effectively within the airline network.

5 Discussion

This study proposes a novel clustering framework, C^4 , which adaptively integrates network topology and node-level covariate information through a data-driven weighting mechanism. The method unifies structure- and covariate-based community detection within a single framework that allows both the tuning parameter α and the number of clusters K to be automatically selected or flexibly specified by the user. Because the covariate similarity matrix \mathbf{S} is normalized to match the scale of the adjacency matrix \mathbf{W} , the tuning parameter α gains a clear and interpretable meaning, in contrast to the CASC algorithm ([Binkiewicz et al., 2017](#)), where such interpretation is not directly available due to the mismatch of scales. Simulation results show that C^4 consistently achieves accurate and stable recovery of

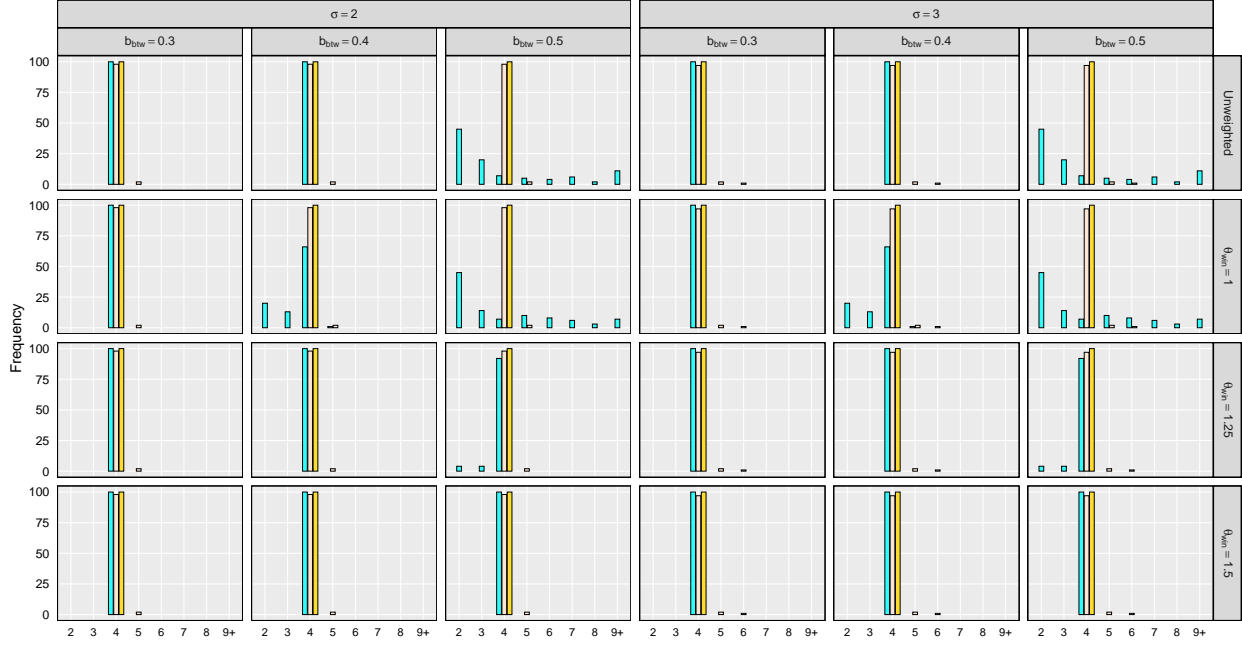
community structures across diverse configurations. The algorithm remains computationally efficient, with a complexity comparable to standard spectral clustering, and scales well to networks with thousands of nodes, making it suitable for practical applications.

Despite these strengths, several limitations and extensions merit future investigation. First, when the covariate information consists of a single categorical variable, the silhouette score may become degenerate, achieving its maximum value of 1 when the clustering is trivially determined by the covariate ($\alpha = 1$). This degeneracy prevents the adaptive selection of α , as the silhouette criterion becomes uninformative under perfectly separable partitions. Alternative selection strategies or penalized objectives that down-weight trivially separable configurations could mitigate this issue. Second, the current implementation relies on a fixed grid search over α and a chosen covariate similarity measure; finer grids or alternative distance metrics may influence performance. Future work could formalize stability diagnostics or develop data-driven procedures for choosing both the similarity function and tuning grid. Third, while C^4 effectively handles weighted networks, further research could examine how heterogeneous degree distributions or extreme weight variability affect clustering results and whether normalization or degree-correction improves robustness. Finally, establishing theoretical guarantees for community recovery and extending the framework to dynamic or multilayer networks would enhance its general applicability.

A Appendix

Figure 4 and 5 present the empirical distributions of the estimated K for $\alpha = 0$, $\alpha = 1$, and C^4 , respectively, across all simulation configurations. It is worth noting that in extreme scenarios where structural signal is severely weak and covariate signal is not strong either (e.g. $b_{\text{btw}} = 0.5$, $K = 8$, $\sigma = 3$, and $n \in \{400, 800\}$, with $\theta_{\text{win}} = 1$ or the unweighted network, corresponding to the first and second rows in the last columns of both panels in Figure 5.), the distribution of K selection for C^4 becomes identical to $\sigma = 1$. In these scenarios, C^4

(a) Network size $n = 400$.



(b) Network size $n = 800$.

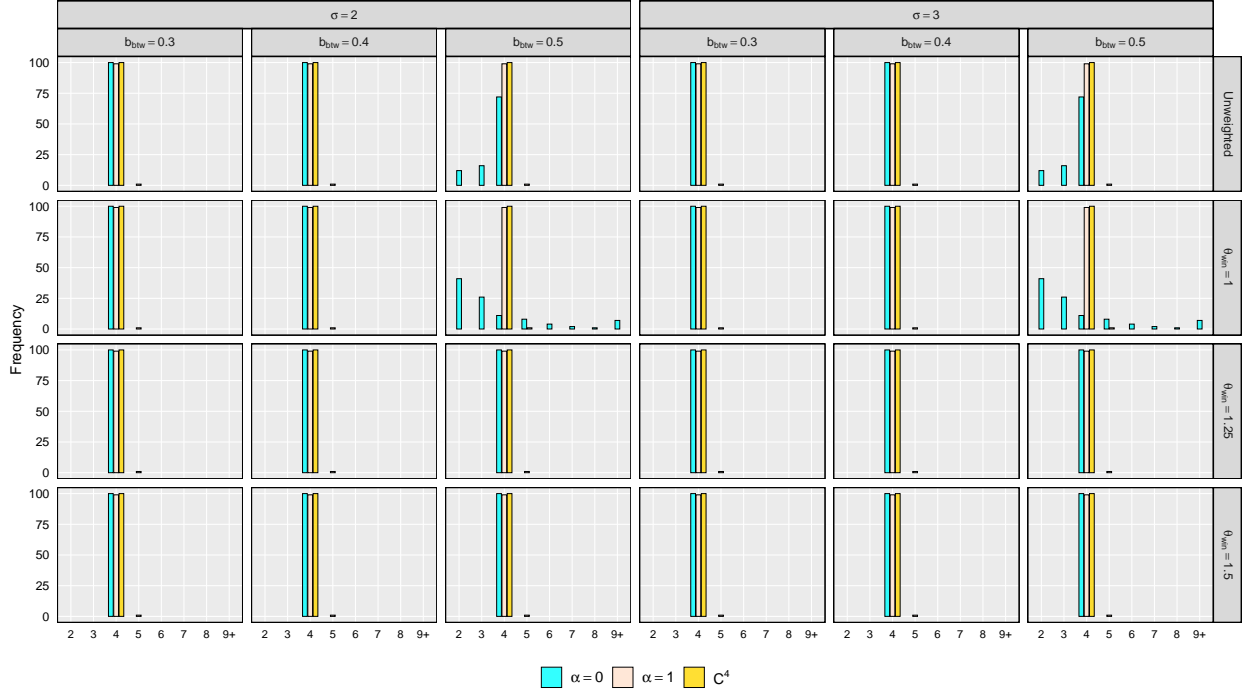
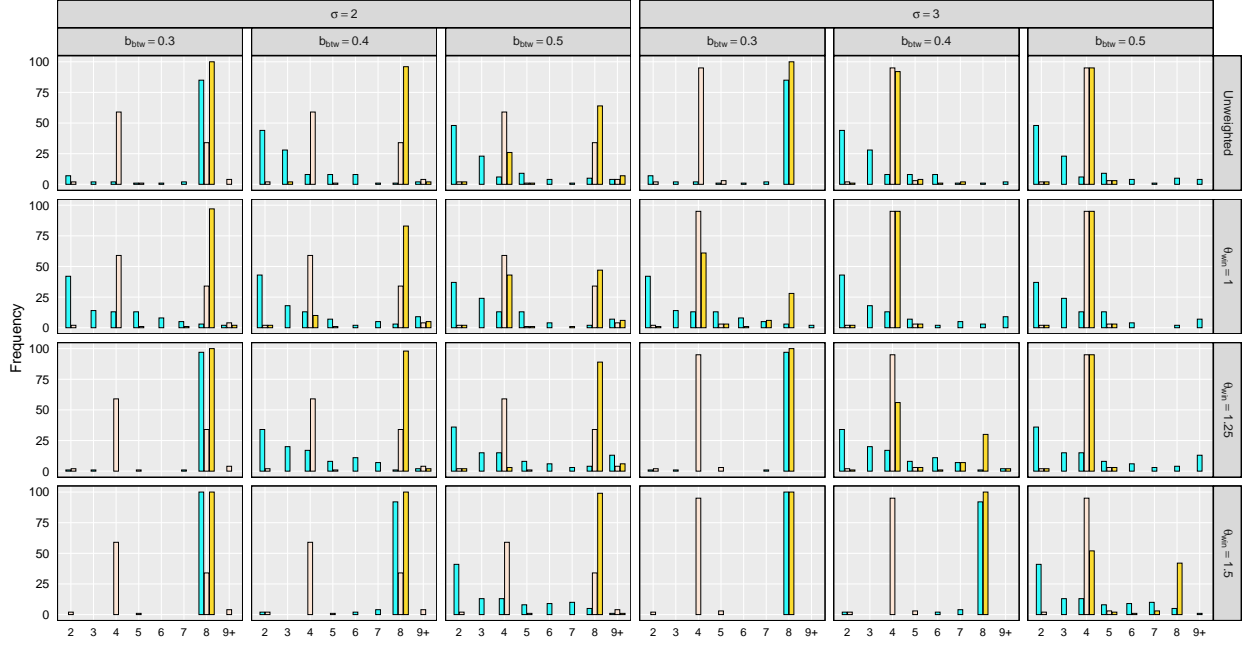


Figure 4: Distribution of the K selection under $K_{\text{true}} = 4$ among all simulation configurations with $n = 400$ (upper) and $n = 800$ (lower).

(a) Network size $n = 400$.



(b) Network size $n = 800$.

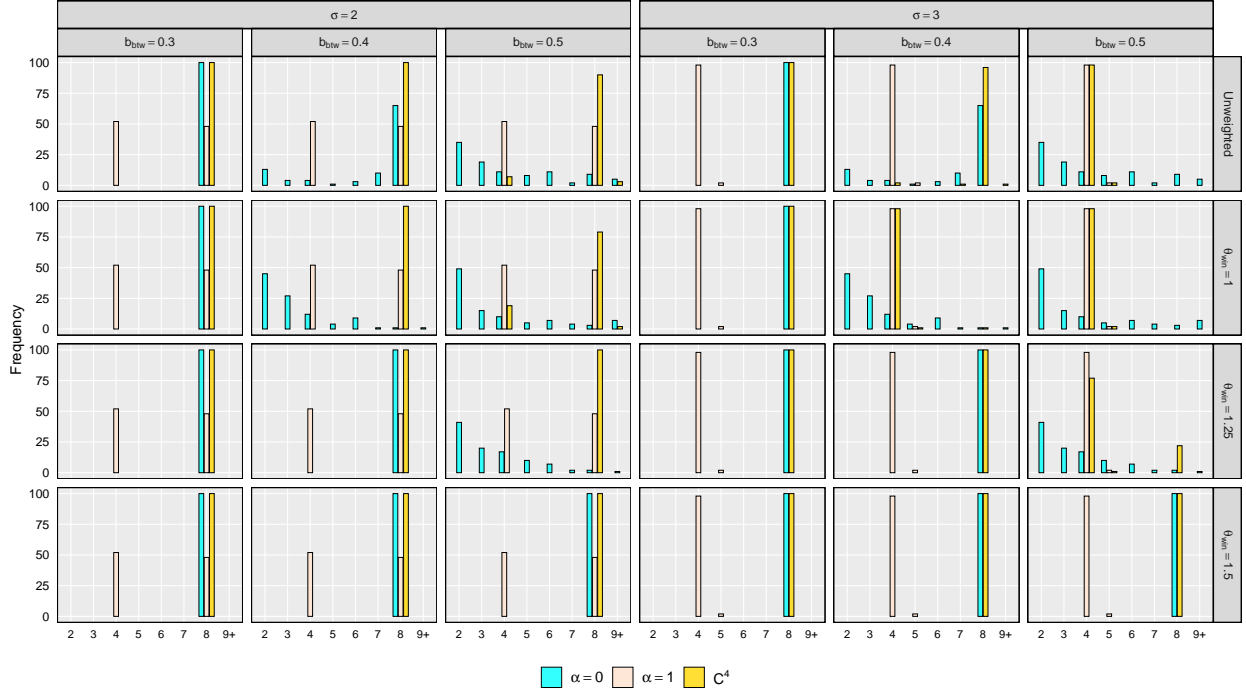


Figure 5: Distribution of the K selection under $K_{true} = 8$ among all simulation configurations with $n = 400$ (upper) and $n = 800$ (lower).

automatically detects that structural information is totally unreliable as noise and selects α to be 1 as the estimated tuning parameter. Although $\alpha = 0$ method occasionally estimates the correct $K = 8$ in these extreme settings, cross-comparison with Figure 2 shows that these rare correct identifications still result in very poor clustering performance. Therefore, C⁴ which relies on covariates only in these scenarios represents a rational adaptation that prioritizes clustering quality over nominally correct but uninformative K identification. However, in real applications, if such extreme scenario happens, users should carefully reassess the data and manually set α range based on domain knowledge to obtain more reliable results.

References

Airoldi, E. M., D. M. Blei, S. E. Fienberg, and E. P. Xing (2008). Mixed membership stochastic blockmodels. *Journal of Machine Learning Research* 9(65), 1981–2014.

Barabási, A.-L., H. Jeong, Z. Néda, E. Ravasz, A. Schubert, and T. Vicsek (2002). Evolution of the social network of scientific collaborations. *Physica A: Statistical Mechanics and its Applications* 311(3–4), 590–614.

Benson, A. R., D. F. Gleich, and J. Leskovec (2016). Higher-order organization of complex networks. *Science* 353(6295), 163–166.

Binkiewicz, N., J. T. Vogelstein, and K. Rohe (2017). Covariate-assisted spectral clustering. *Biometrika* 104(2), 361–377.

Blondel, V. D., J.-L. Guillaume, R. Lambiotte, and E. Lefebvre (2008). Fast unfolding of communities in large networks. *Journal of Statistical Mechanics: Theory and Experiment* 2008(10), P10008.

Chen, J. and P. Zhang (2022). Clustering US states by time series of COVID-19 new case counts in the early months with non-negative matrix factorization. *Journal of Data Science* 20(1), 79–94.

Chung, F. R. K. (1997). *Spectral Graph Theory*. Providence, RI: American Mathematical Society.

Contisciani, M., E. A. Power, and C. De Bacco (2020). Community detection with node attributes in multilayer networks. *Scientific Reports* 10(1), 15736.

Dudek, A. (2020). Silhouette index as clustering evaluation tool. In *Classification and Data Analysis (SKAD 2019)*, pp. 19–33. Cham, Switzerland: Springer.

Fortunato, S. (2010). Community detection in graphs. *Physics Reports* 486(3–5), 75–174.

Frey, B. J. and D. Dueck (2007). Clustering by passing messages between data points. *Science* 315(5814), 972–976.

Girvan, M. and M. E. J. Newman (2002). Community structure in social and biological networks. *Proceedings of the National Academy of Sciences of the United States of America* 99(12), 7821–7826.

Handcock, M. S., A. E. Raftery, and J. M. Tantrum (2007). Model-based clustering for social networks. *Journal of the Royal Statistical Society: Series A (Statistics in Society)* 170(2), 301–354.

Hu, Y. and W. Wang (2023). *CASCORE: Covariate Assisted Spectral Clustering on Ratios of Eigenvectors*. Southern Methodist University. R package version 0.1.2.

Januzaj, Y., E. Beqiri, and A. Luma (2023). Determining the optimal number of clusters using silhouette score as a data mining technique. *International Journal of Online and Biomedical Engineering* 19(4), 174–182.

Ji, P., J. Jin, Z. T. Ke, and W. Li (2022). Co-citation and co-authorship networks of statisticians. *Journal of Business & Economic Statistics* 40(2), 469–485.

Lin, W., X. Kong, P. S. Yu, Q. Wu, Y. Jia, and C. Li (2012). Community detection in incomplete information networks. In A. Mille, F. Gandon, and J. Misselis (Eds.),

Proceedings of the 21st International Conference on World Wide Web (WWW'12), New York, NY, pp. 341–350. Association for Computing Machinery.

Louit, S., E. Clark, A. Gelbard, N. Vivek, J. Yan, and P. Zhang (2025). CALF-SBM: A covariate-assisted latent factor stochastic block model. *Physica A: Statistical Mechanics and its Applications* 667, 130536.

Newman, M. E. J. (2006). Modularity and community structure in networks. *Proceedings of the National Academy of Sciences of the United States of America* 103(23), 8577–8582.

Newman, M. E. J. and A. Clauset (2016). Structure and inference in annotated networks. *Nature Communications* 7(1), 11863.

Newman, M. E. J. and M. Girvan (2004). Finding and evaluating community structure in networks. *Physical Review E* 69(2), 026113.

Ng, A. Y., M. I. Jordan, and Y. Weiss (2002). On spectral clustering: Analysis and an algorithm. In T. G. Dietterich, S. Becker, and Z. Ghahramani (Eds.), *Proceedings of the 15th International Conference on Neural Information Processing Systems (NIPS'01)*, Cambridge, MA, pp. 849–856. MIT Press.

Ouyang, G., D. K. Dey, and P. Zhang (2021). Clique-based method for social network clustering. *Journal of Classification* 37(1), 254–274.

Ouyang, G., D. K. Dey, and P. Zhang (2023). A mixed-membership model for social network clustering. *Journal of Data Science* 21(3), 508–522.

Pons, P. and M. Latapy (2005). Computing communities in large networks using random walks. *Journal of Graph Algorithms and Applications* 10(2), 191–218.

Radicchi, F., C. Castellano, F. Cecconi, V. Loreto, and D. Parisi (2004). Defining and identifying communities in networks. *Proceedings of the National Academy of Sciences of the United States of America* 101(9), 2658–2663.

Raghavan, U. N., R. Albert, and S. T. Kumara (2007). Near linear time algorithm to detect community structures in large-scale networks. *Physical Review E* 76(3), 036106.

Rand, W. M. (1971). Objective criteria for the evaluation of clustering methods. *Journal of the American Statistical Association* 66(336), 846–850.

Rosvall, M. and C. T. Bergstrom (2008). Maps of random walks on complex networks reveal community structure. *Proceedings of the National Academy of Sciences of the United States of America* 105(4), 1118–1123.

Rousseeuw, P. J. (1987). Silhouettes: A graphical aid to the interpretation and validation of cluster analysis. *Journal of Computational and Applied Mathematics* 20(1), 53–65.

Shahapure, K. R. and C. Nicholas (2020). Cluster quality analysis using silhouette score. In G. Webb, Z. Zhang, V. S. Tseng, G. Williams, M. Vlachos, and L. Cao (Eds.), *Proceedings of IEEE 7th International Conference on Data Science and Advanced Analytics (DSAA)*, Los Alamitos, CA, USA, pp. 747–748. IEEE Conference Publishing Services.

Shen, L., A. Amini, N. Josephs, and L. Lin (2025). Bayesian community detection for networks with covariates. *Bayesian Analysis* 20(3), 735–762.

Shi, J. and J. Malik (2000). Normalized cuts and image segmentation. *IEEE Transactions on Pattern Analysis and Machine Intelligence* 22(8), 888–905.

Sporns, O. and R. F. Betzel (2016). Modular brain networks. *Annual Review of Psychology* 67, 613–640.

Tallberg, C. (2004). A Bayesian approach to modeling stochastic blockstructures with covariates. *Journal of Mathematical Sociology* 29(1), 1–23.

von Luxburg, U. (2007). A tutorial on spectral clustering. *Statistics and Computing* 17(4), 395–416.

Wang, S., J. G. Yabes, and C.-C. H. Chang (2021). Hybrid density- and partition-based clustering algorithm for data with mixed-type variables. *Journal of Data Science* 19(1), 15–36.

Xu, S., Y. Zhen, and J. Wang (2023). Covariate-assisted community detection in multi-layer networks. *Journal of Business & Economic Statistics* 41(3), 915–926.

Yan, B. and P. Sarkar (2021). Covariate regularized community detection in sparse graphs. *Journal of the American Statistical Association* 116(534), 734–745.

Zhang, Y., R. Pan, H. Wang, and H. Su (2023). Community detection in attributed collaboration network for statisticians. *Stat* 12(1), e507.